SAND2015-8135PE

Exceptional service in the national interest

Sandia National Laboratories

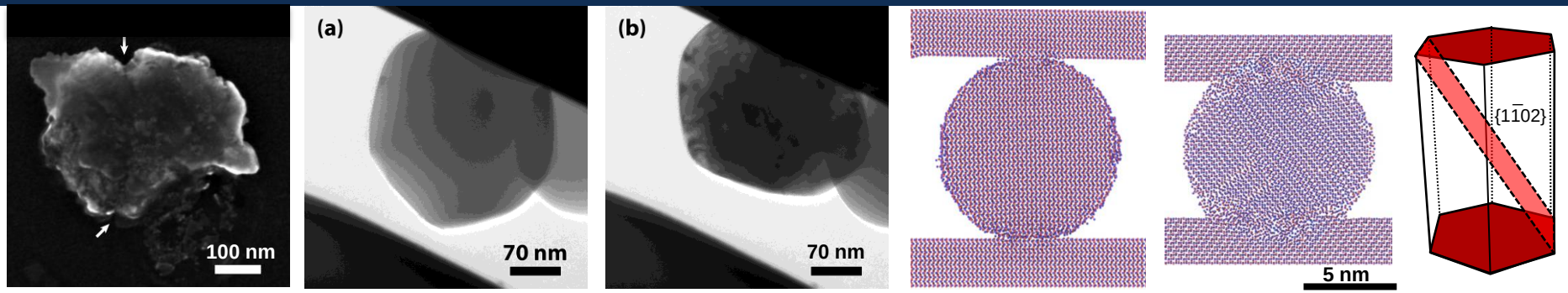

Deformation of Alumina Particles in Compression – Basis for a Room Temperature Ceramic Coating Deposition

Pylin Sarobol, Michael Chandross, Daniel C. Bufford, Khalid Hattar, Paul G. Kotula, Brad L. Boyce, Jay D. Carroll, Aaron C. Hall, and William M. Mook

National Lab Day @ Purdue University, Oct 6-7, 2015

U.S. DEPARTMENT OF ENERGY | NNSA National Nuclear Security Administration

Sandia National Laboratories is a multi-program laboratory managed and operated by Sandia Corporation, a wholly owned subsidiary of Lockheed Martin Corporation, for the U.S. Department of Energy's National Nuclear Security Administration under contract DE-AC04-94AL85000. SAND2015-3704C

Motivation

- Bulk materials with high degrees of covalent/ionic bonding, e.g. ceramics, typically undergo brittle fracture when strained.
  - a combination of limited fracture toughness and preexisting flaws.
  - The role of pre-existing flaws and defects can evolve as the characteristic length scale of materials decrease (e.g. micro-pillars and particles) [1-14].
  - In bulk ceramics →crack initiation sites.
- **At small length scales, significant plasticity observed in ceramic single crystals at room temperatures.**
  - Low strain rates → dislocation slip and shape change
    - compressed sapphire micro-pillars [10], particles [16], and confined zones underneath an indenter [36] at RT.
  - High strain rates → aerosol deposition (AD)
    - < 2 μm particles are accelerated to high velocity (200-600 m/s) by pressurized gas, impacted, deformed, and consolidated on the substrates under vacuum [16-24].
- Room temperature plasticity in ceramics at small length scale gave insights into future development of alternative ceramic forming technology and high strength/high toughness functional ceramics.
- The focus of this study is to better understand the deformation behavior observed in small-scale, compressed ceramic particles, specifically sapphire or α-Al_2O_3 and how they play a role in making AD coatings.

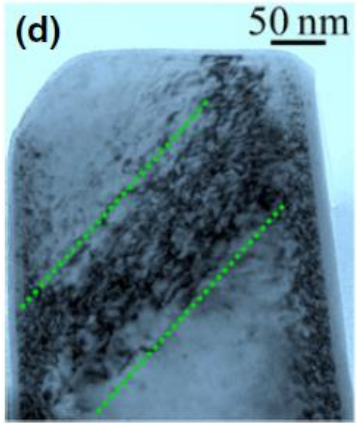

Dislocations on {001} planes in compressed ZrC pillar from S. Kiani, *et al. J. Am. Ceram. Soc.*, 2015:98:2313

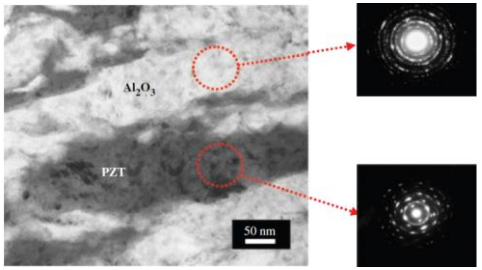

AD Al2O3 and PZT composite film from J. Akedo. *J. Am. Ceram. Soc.,* 2006:89:1834

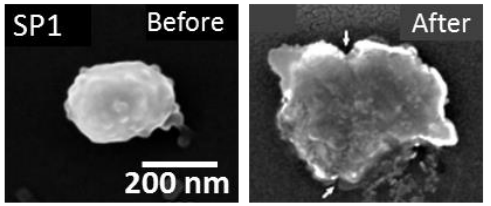

Compressed sapphire particle from P. Sarobol, *et al.*, *JTST.*, 2016:25

Motivation

Aerosol Deposition (AD) enables materials integration.

- Ceramics are conventionally processed at 2000°C.
- AD process at room temperature (RT) in vacuum
  - sub-micron particles accelerated to high velocity by pressurized gas, impacted, consolidated to form a film.
- Similar AD ceramic film microstructures
  - sub-micron particles undergo *plastic deformation*
  - break up into *small crystallites* (20-75 nm)[1-3]
  - planar *defects* and *amorphous regions*[4].

Particle deformation/bonding not well understood

- Common deformation mechanisms exist.
- Examine sub-micron ceramic particles RT deformation as a building block for AD coatings.

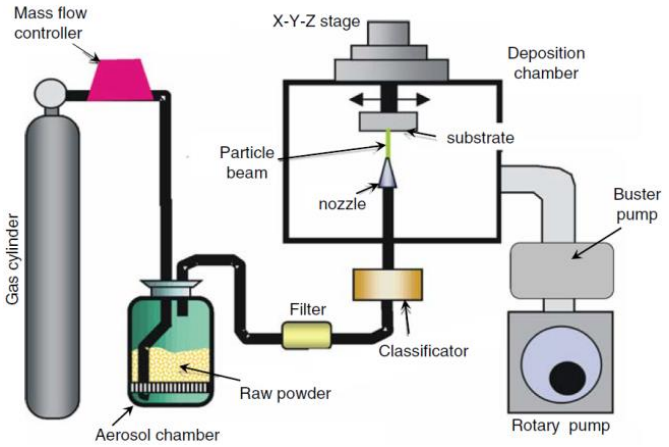

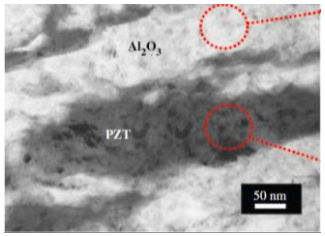

AD process and coatings from Akedo *J. Am. Ceram. Soc.*, 2006;89:1834

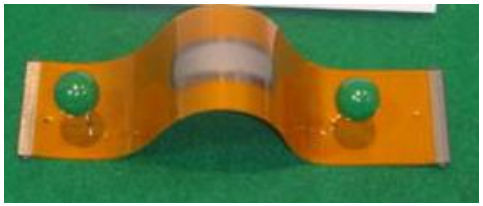

AD Flexible electronics from J. Akedo. *JTTEE5.,* 2007:17:181

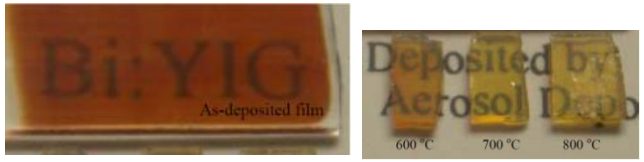

AD magnetic films from Mizoguchi et al. J. Magnetic Soc Japan 2006:30;659

[1] Akedo, J. and Ogiso, H., *JTST*, Vol. 17, (2008), pp. 181-198.
[2] Akedo, J., *JTTEE5*, Vol. 17, (2007), pp. 181-198.
[3] Akedo, J. *J. Am. Ceram. Soc.*, Vol. 89, (2006), pp. 1834-1839.
[4] Park, H. *et al.* Scripta Materialia, 2015.

Previous work – P. Sarobol, et al., *JTST*., 2016:**25**

DOI 10.1007/s11666-015-0295-2

Sandia National Laboratories

- Performed micro-compression on 3.0 µm and 0.3 µm Al_2O_3 particles
- Micron sized particles - brittle fracture
  - Absorbed strain energy density before fracture **107 ± 69 MJ/m³**
  - Strain before fracture **5.5 ± 1%**
- Sub-micron sized particles - substantial plastic deformation before fracture.
  - Absorbed strain energy density before fracture **630 ± 238 MJ/m³**
  - Strain before fracture **18 ± 9 %**
  - Deformable sub-micron sized particles = AD coating building block

- **6x** higher strain energy density
  - dislocation nucleation
- **3x** higher accumulated strain

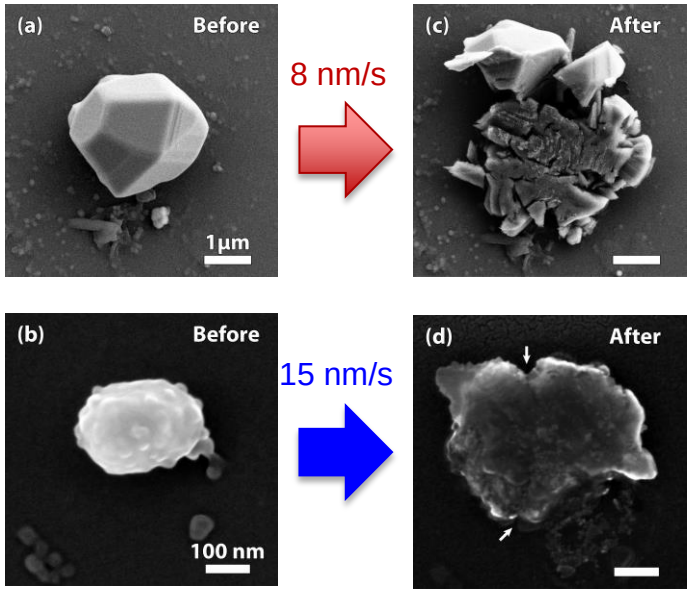

	Micron	Sub-micron
# Pre-existing Defects	High	Moderate
Energy Density Input	Low	Moderate
Governing Mechanism(s)	Fracture	Plasticity + Fracture
Response to Compression	Crack initiation & Propagation	Dislocation nucleation, slip, crack initiation & propagation

Sub-micron sized Al_2O_3 response to compression
– *In Situ* TEM micro-compression
– Molecular Dynamics Simulation

In Situ TEM Compression

In Situ Micro-Compression[5] – 300 nm particles

- Single crystal, ultra pure 300 nm sapphire (α-Al_2O_3) particles.
- A Hysitron PI95 TEM Picoindenter with a 1 µm diameter flat punch tip and the a JEOL 2100 LaB_6 TEM[7] at 200 kV were used.
- Compression done in ***open loop*** mode with the loading rate of 10 µN/s (approx. **< 2 nm/s** displ rate). Images taken at 15 fps.

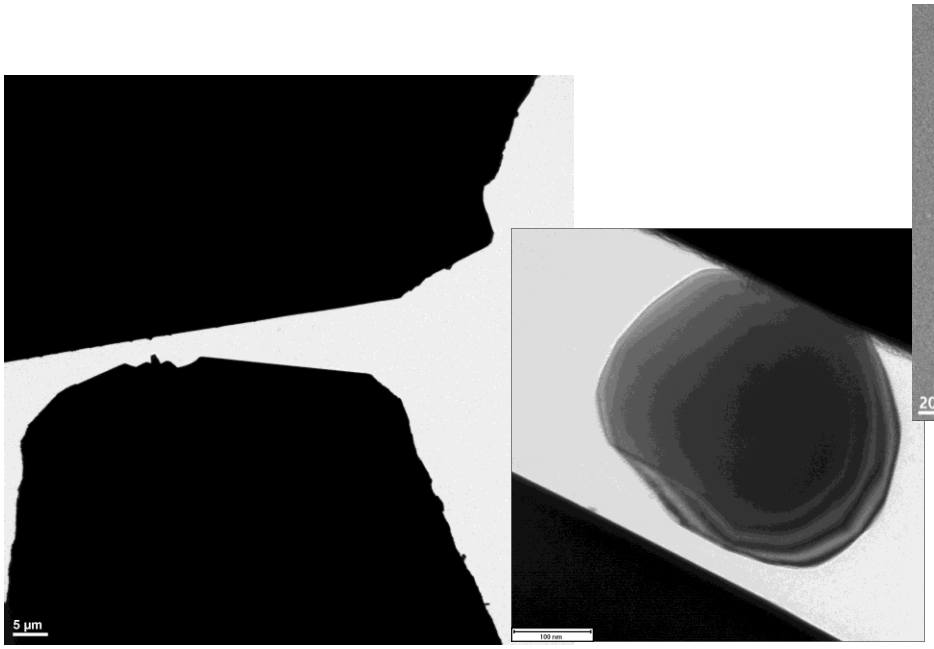

***In situ* TEM micro-compression on 0.3µm particle**

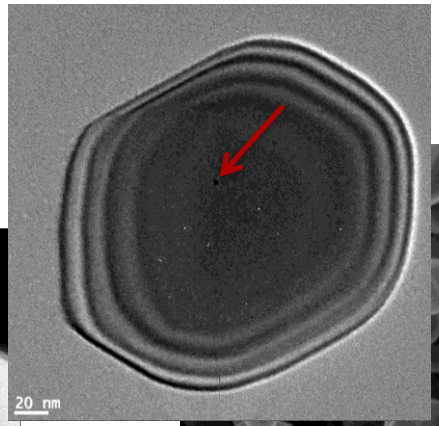

Bright field TEM image of a 300 nm particle oriented on the [001] zone axis.

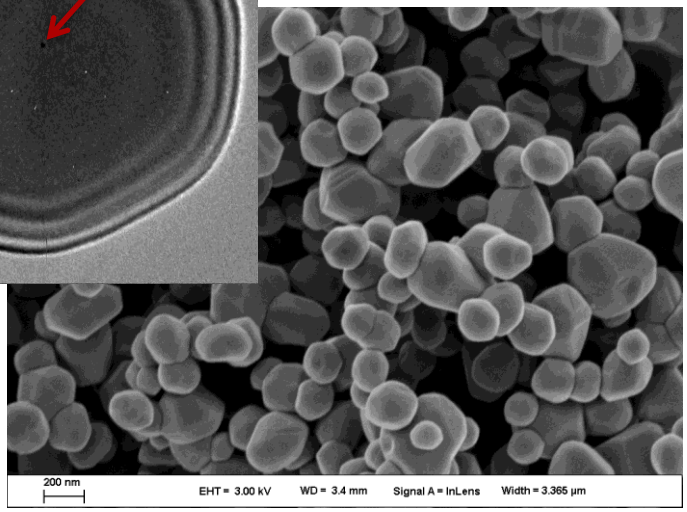

SE SEM image of the 300 nm

[5] Sarobol, P., *et al*., *SAND2014-18127*, (2014).
[6] Hysitron I (2013) SEM Picoindenter User Manual. Revision 9.3.0913 edn.
[7] Hattar, K., et al., Nuclear Instruments and Methods in Physics Research B. Vol. 338, (2014), pp. 56–65.

In Situ TEM Compression

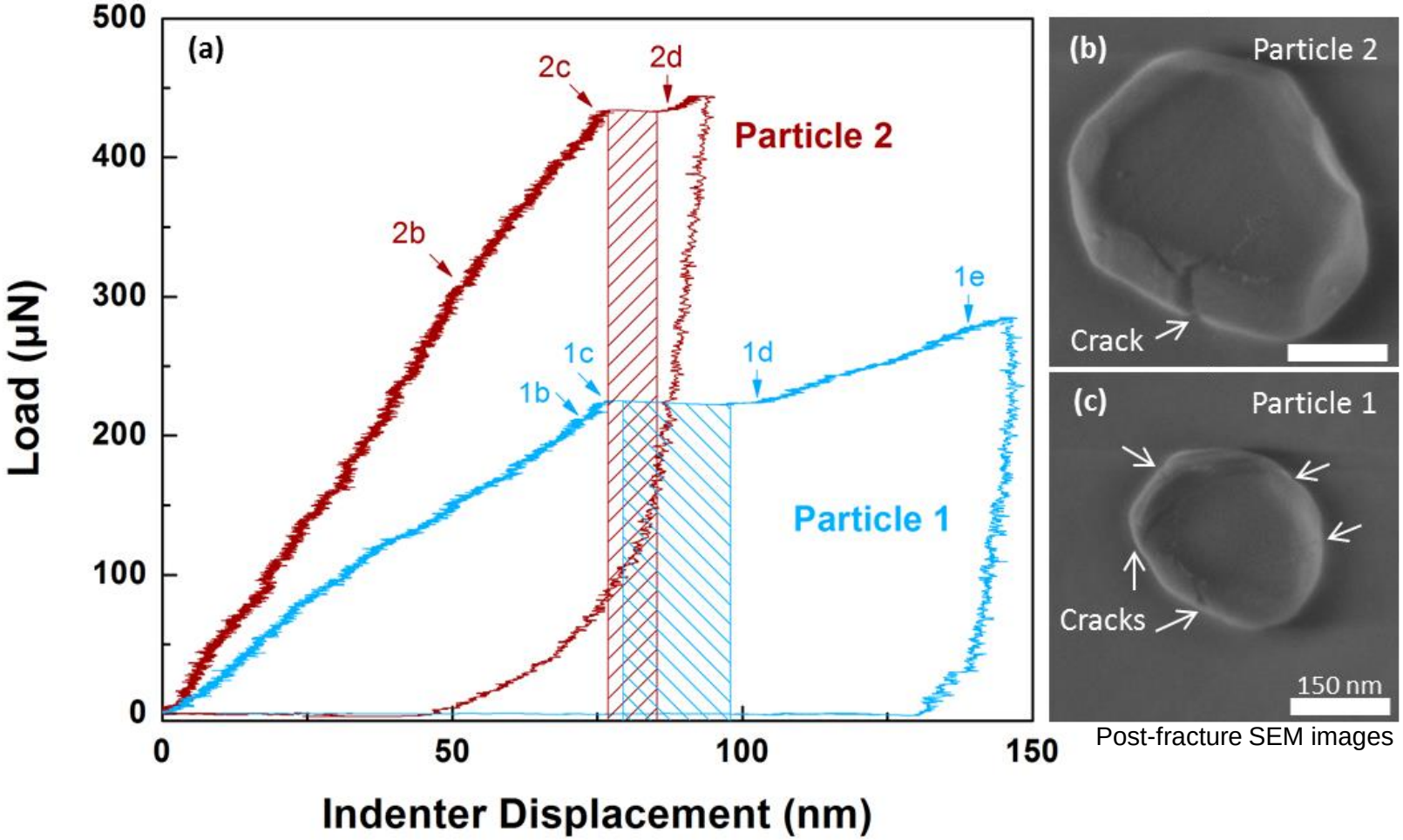

Post-fracture SEM images

- Elastic to Plastic transitions are unclear. Seemed to happen much earlier in the loading (first 5-10 nm displacement). Absence of concavity and linearity of the curves were surprising.
- G_C values for Particle 1 and 2 are 45 J/m^2 and 17 J/m^2, respectively. Values within the calculated range of orientation-dependent G_C of single crystal alumina of 16 - 65 J/m^2 [47].

In Situ TEM Compression – P1

Diameter ~ 0.24 µm, Open loop, Strain rate ~ 0.009 s^{-1}

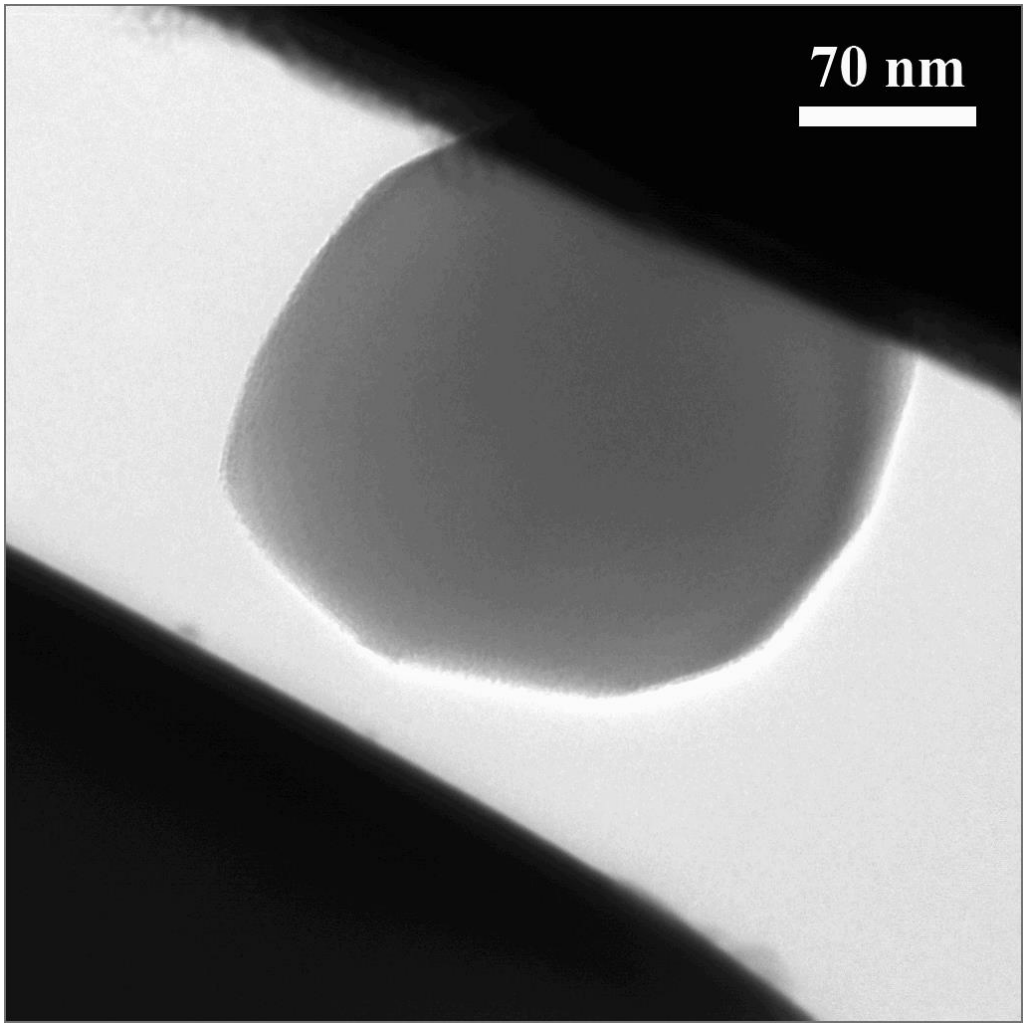

Large displacement gain at a constant load ("burst") corresponds to particle fracture.

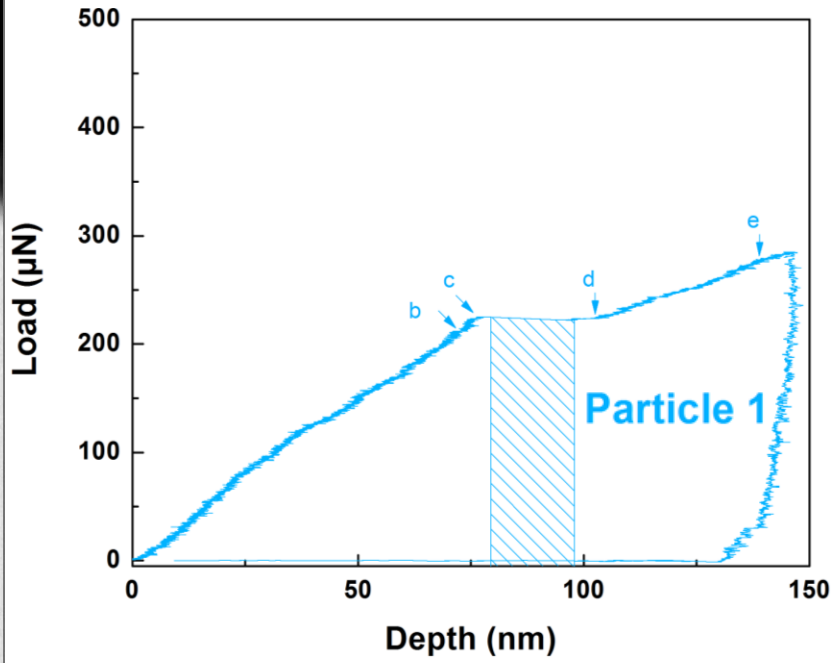

In Situ TEM Compression – P1

Zone axis near [$\bar{9}\,\bar{9}$ 18 6]

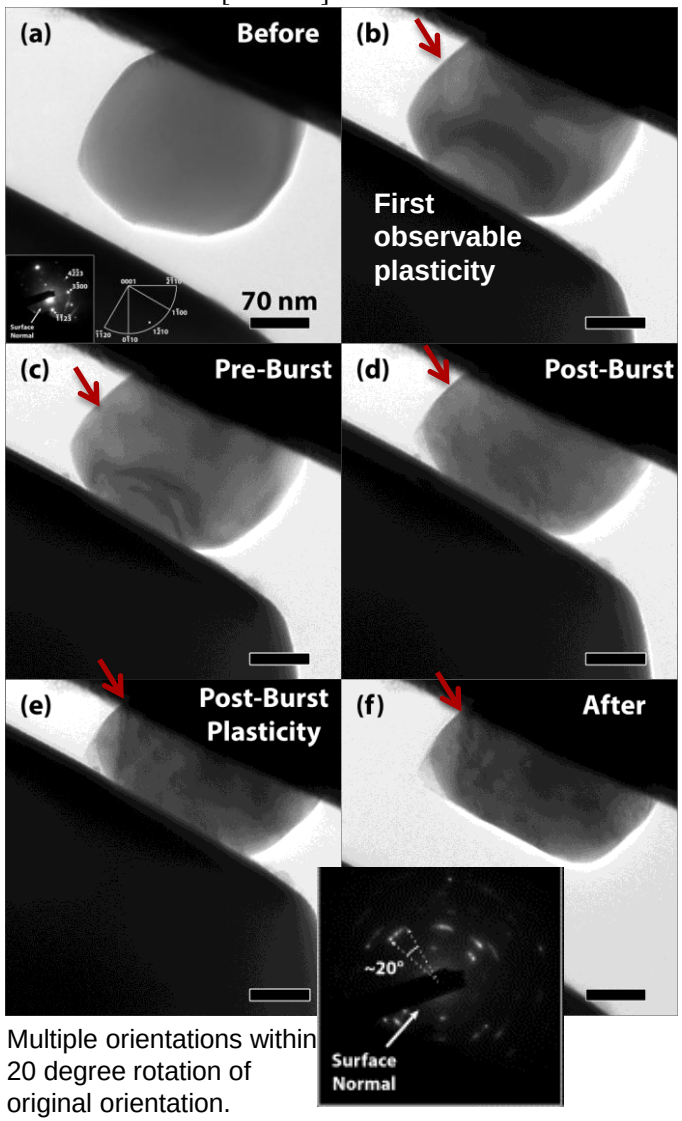

Multiple orientations within 20 degree rotation of original orientation.

- Strain energy release rate = 45 J/m^2

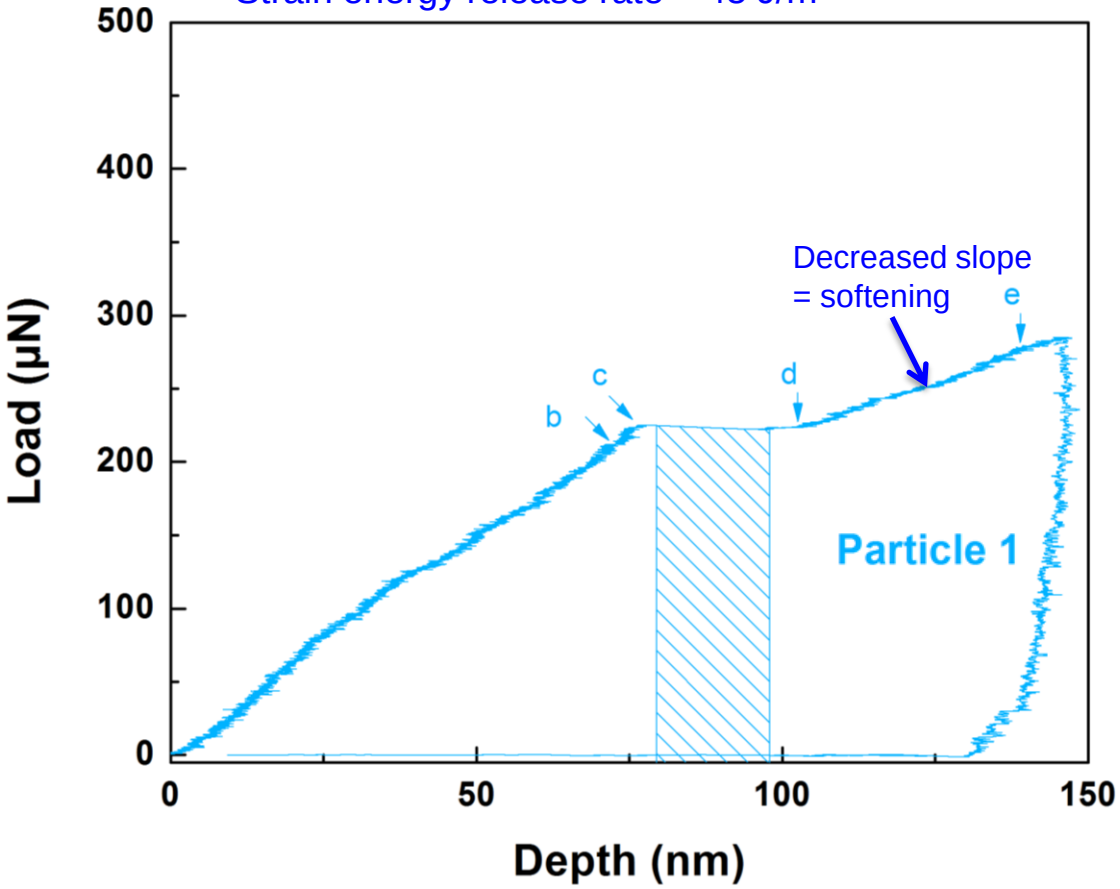

- Pre-burst plasticity: small regime with low dislocation activity.
- **Crack nucleation and propagation** leading to through-particle fracture.
- Post-burst plasticity: high dislocation activities, change in deformation mechanism as indicated by lower slope.
- **Mosaicity** with a 20 degree orientation spread.

In Situ TEM Compression – P2

Diameter ~ 0.38 µm, Open loop, Strain rate ~0.005 s^{-1}

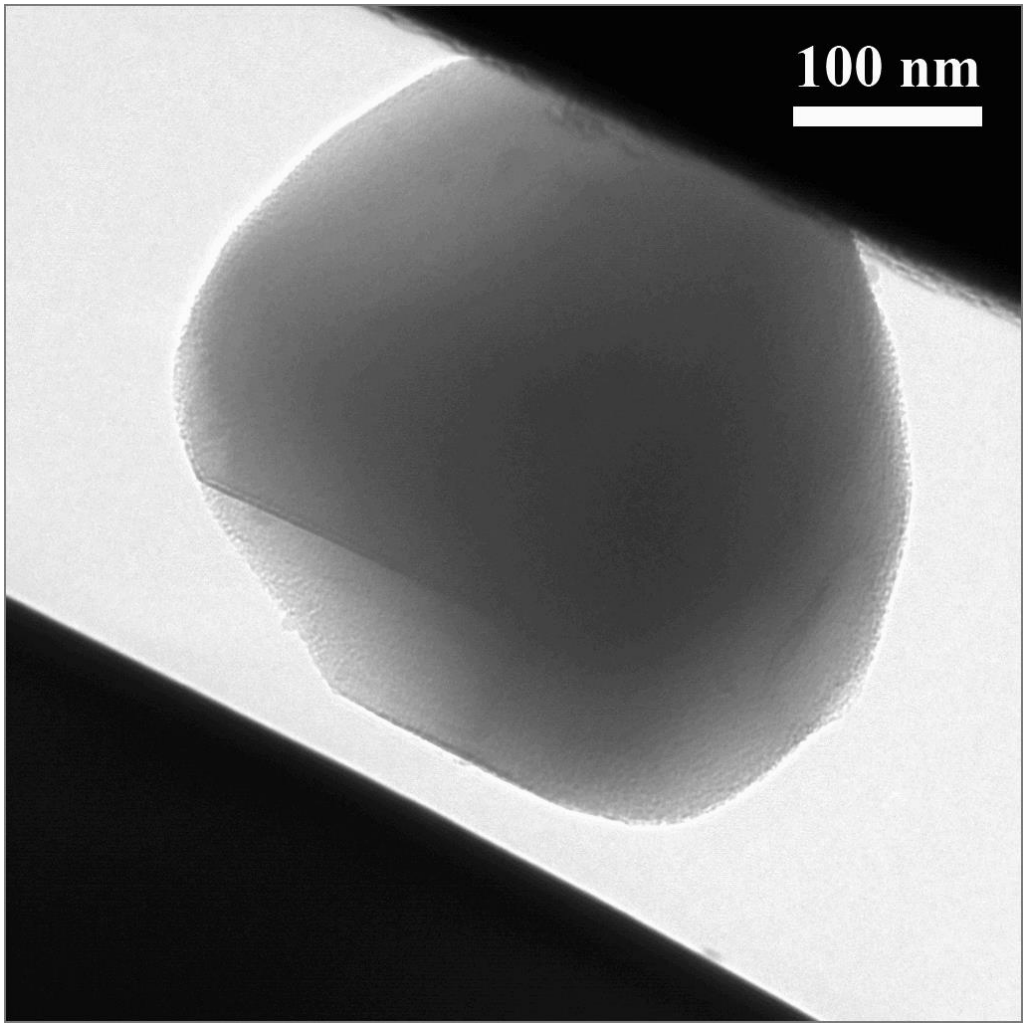

Large displacement gain at a constant load ("burst") corresponds to particle fracture.

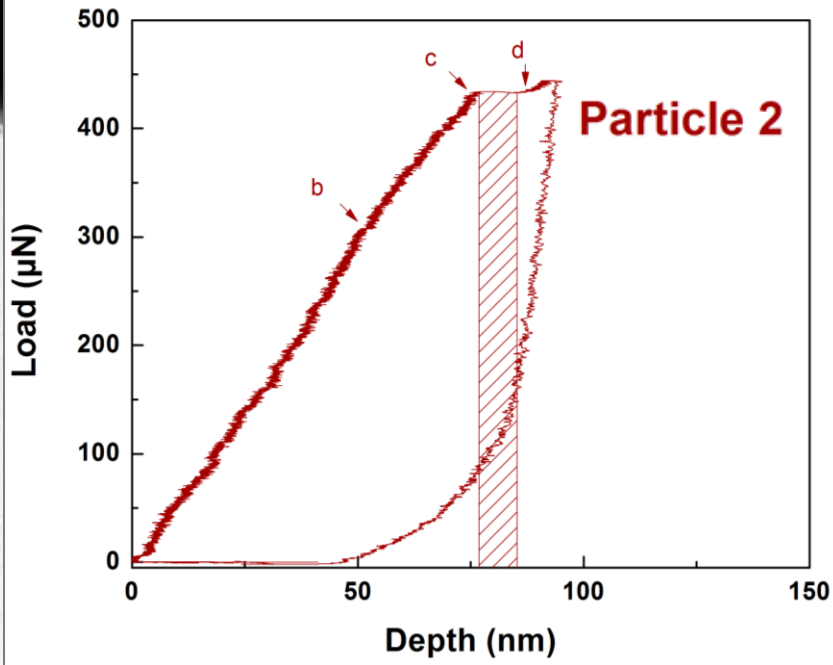

In Situ TEM Compression – P2

Sandia National Laboratories

Zone axis near $[\bar{2}\ 5\ \bar{3}\ 2]$

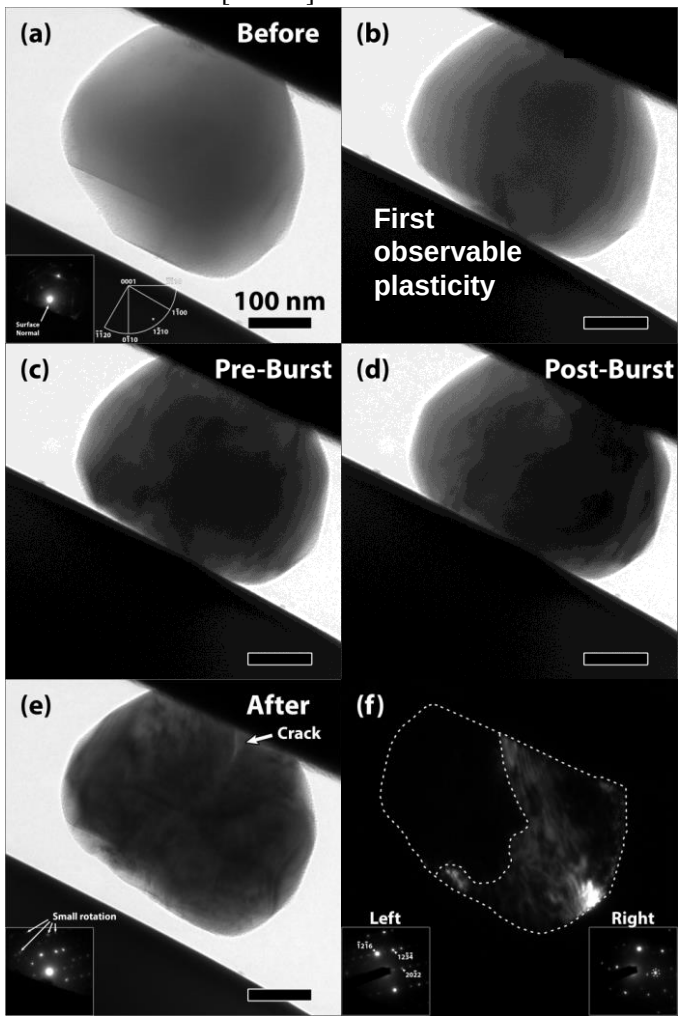

Two halves related by slight rotation, both near $[\bar{1}\ 2\ 1\ 6]$ zone axis

- Strain energy release rate = 17 J/m^2

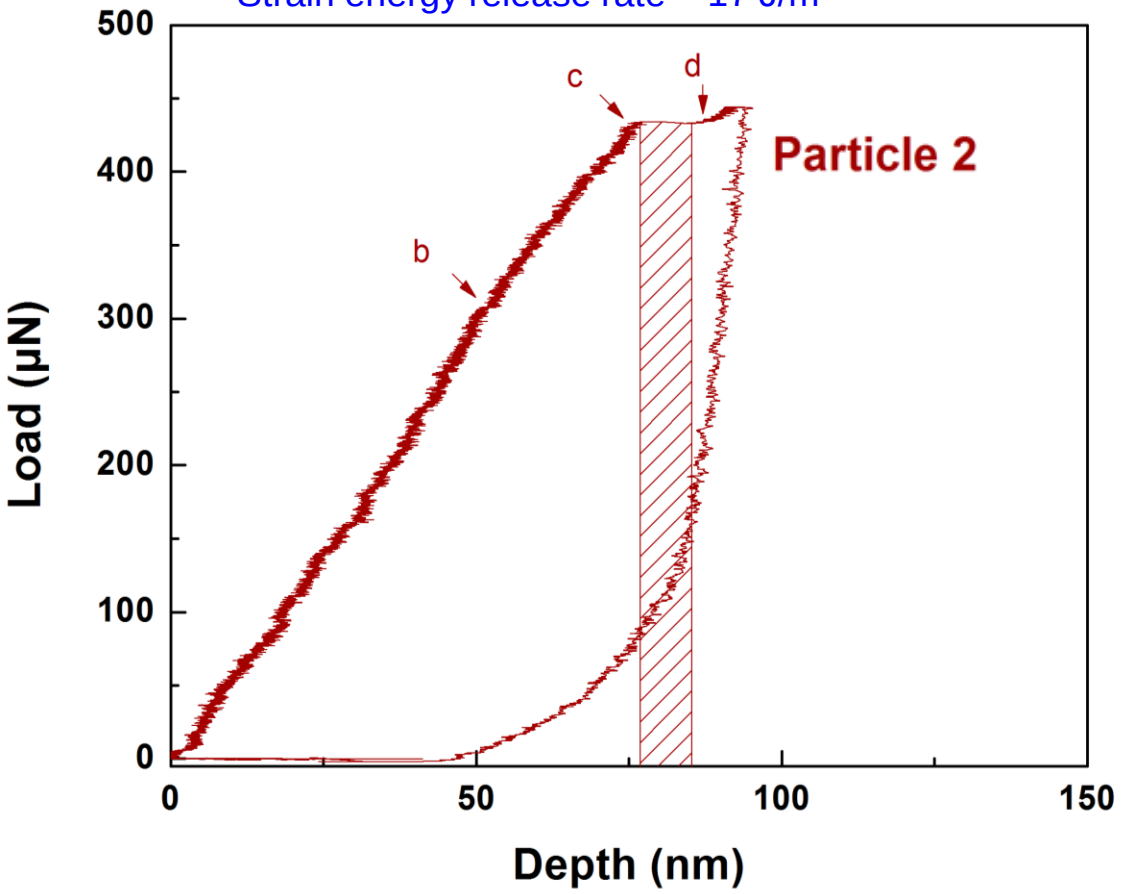

- Pre-burst plasticity: large regime with **high dislocation activity** (nucleation and moving through particle).
- **Crack nucleation and propagation** leading to through-particle fracture.

Simulated Particle Compression

Molecular Dynamics Simulations – 10 nm nanoparticles (NPs)

- MD allows identification of dislocations, slip planes, and particle fracture.
- Long computing time to simulate size > 50 nm (~36 million atoms)
- Simulating 10 nm sapphire nanoparticle (NP) (~300,000 atoms)
- A force-field for ceramics, developed by Garofalini[8].
- NPs were compressed (by ~1/3 of the initial diameter) between sapphire (single crystal α-Al_2O_3) walls at a constant velocity of **20 m/s**. **"Displacement control"**.

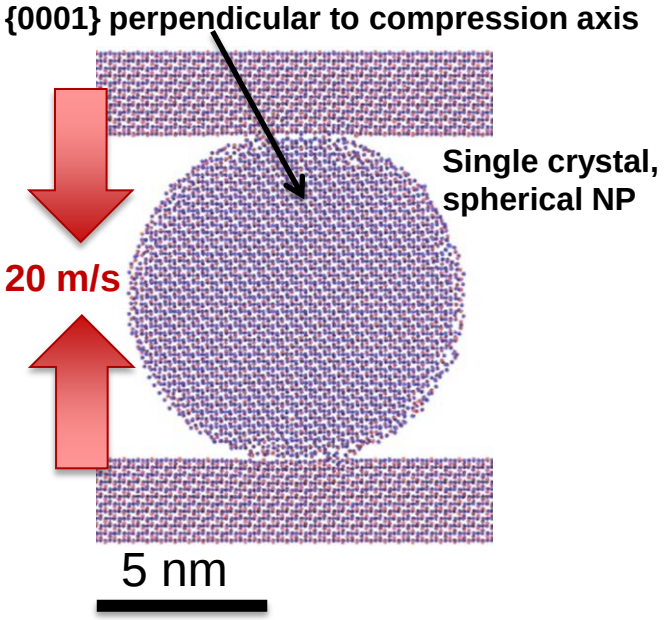

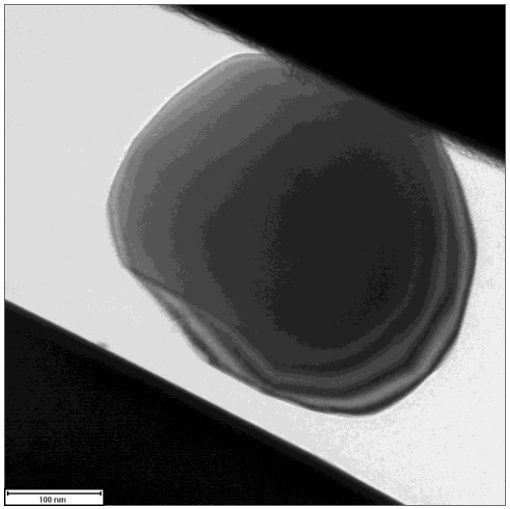

Single crystal, faceted, 300 nm diameter particle

In situ **TEM micro-compression on 0.3μm particle**

[8] Blonski, S. and Garofalini, S. H., *J. Phys. Chem.*, Vol. 100, (1996), pp. 2201-2205.

MD Simulation Results

10 nm diameter, defect-free, single crystal α-alumina, compression axis ⊥ (0001)
20 m/s → dislocation nucleation and glide on Rhombohedral planes then fracture

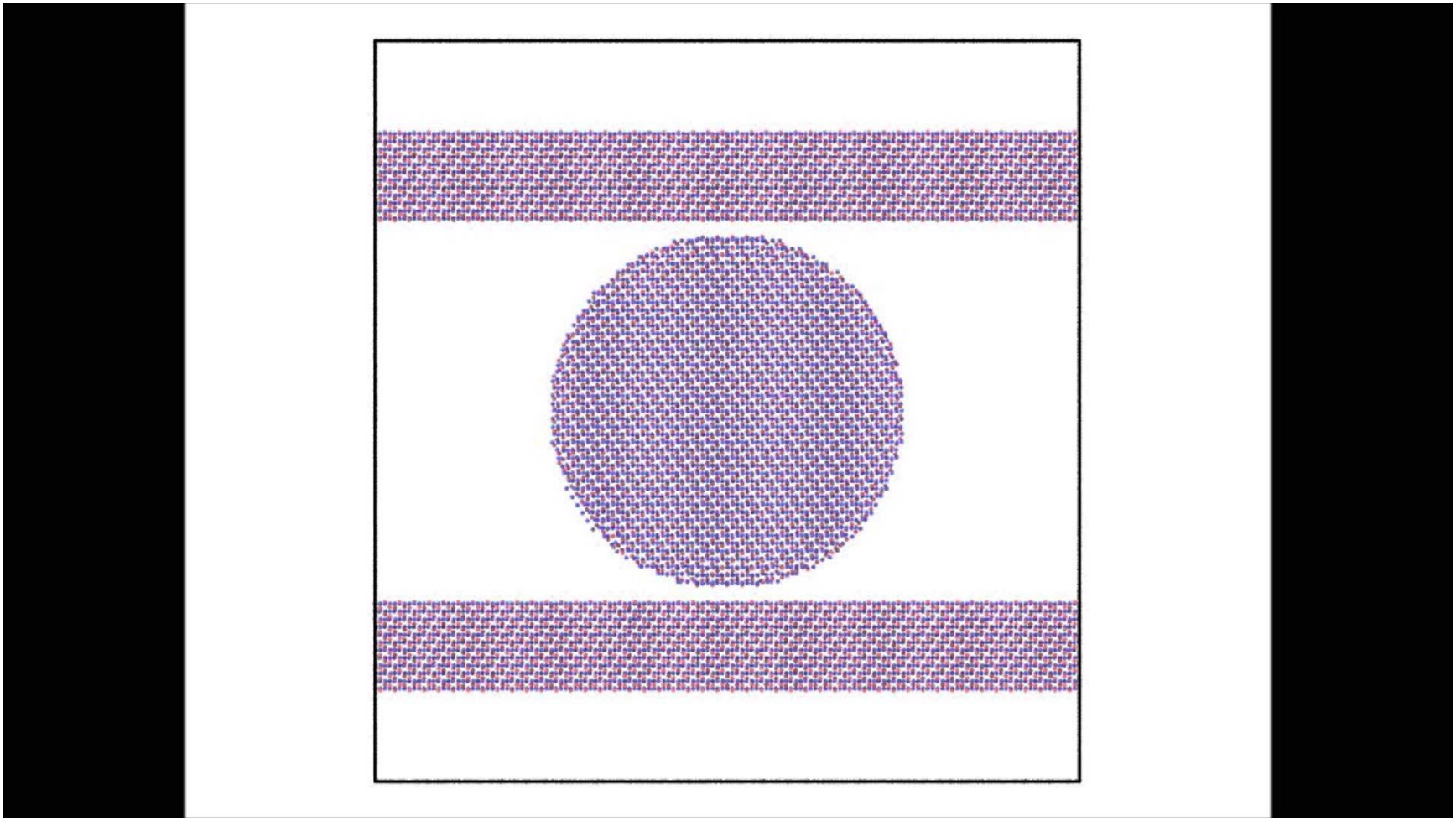

MD Simulation Results

Dislocation plasticity precedes fracture.

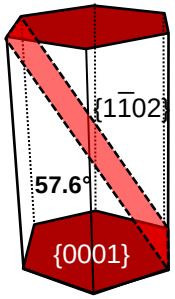

Primary dislocations nucleate at contact points. Then, move through particle on rhombohedral planes

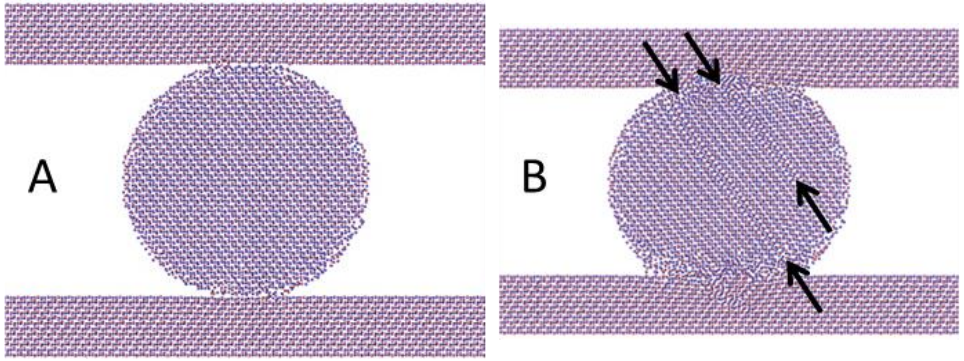

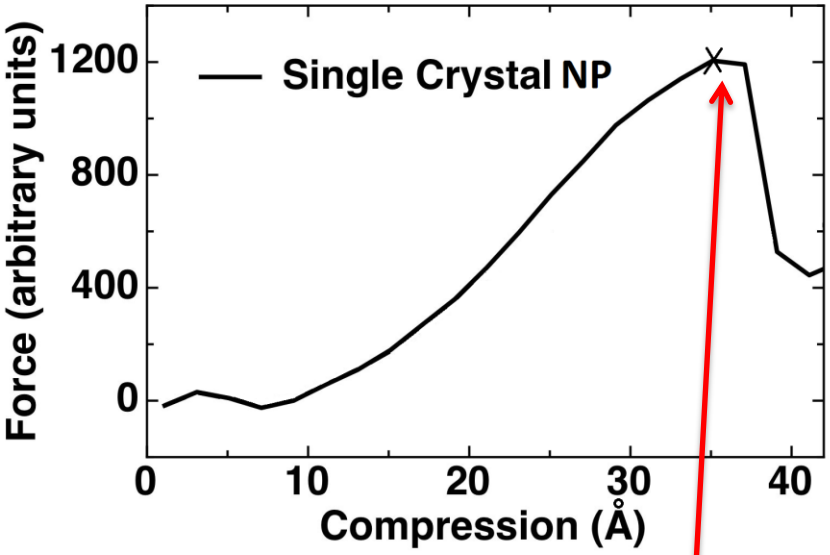

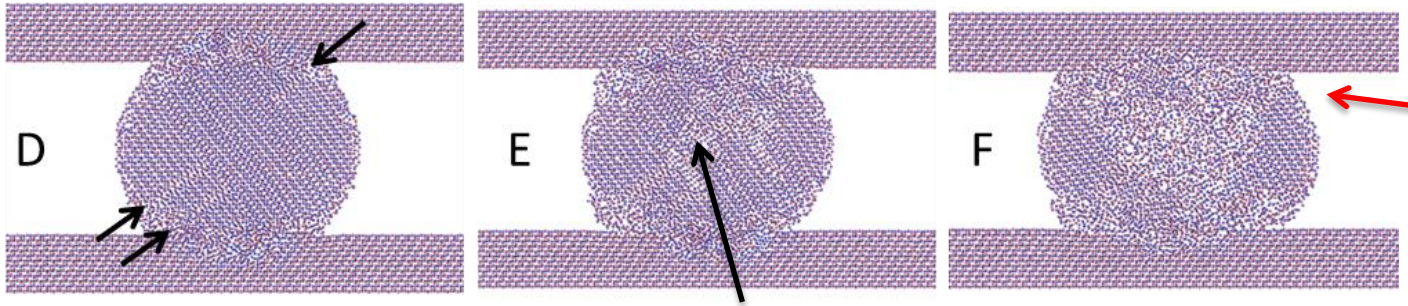

Force drop corresponds to particle fracture

Secondary dislocations nucleate and move through particle on rhombohedral planes, terminating at the primary dislocation planes

Void Initiation

Fracture

Conclusions

- The findings from *in situ* TEM micro-compression experiments and molecular dynamic simulations agree well:
  - Dislocation plasticity precedes fracture in compressed small sapphire particles at RT.
  - Range of responses to compression includes
    - Dislocation nucleation, slip, movement
    - Significant shape change
    - Orientation spread (mosaicity)
    - Fracture
- Use info to inform feedstock preparation, aerosol deposition parameters, and particle-particle bonding in the consolidated coatings.
- Room temperature plasticity in ceramics at small length scale gave insights into future development of alternative ceramic forming technology and high strength/high toughness functional ceramics.

References

1A.R. Beaber, J.D. Nowak, O. Ugurlu, W.M. Mook, S.L. Girshick, R. Ballarini, W.W. Gerberich, *Philos. Mag.*, **91**, 1179 (2011).
2W.W. Gerberich, J. Michler, W.M. Mook, R. Ghisleni, F. Östlund, D.D. Stauffer, and R. Ballarini, *J. Mater. Res.*, **24**, 898 (2009).
3W.W. Gerberich, W.M. Mook, M.J. Cordill, C.B. Carter, C.R. Perrey, J.V. Heberlein, and S.L. Girshick, *Int J Plasticity*., **21**, 2391 (2005).
4F. Östlund, K. Rzepiejewska-Malyska, K. Leifer, L.M. Hale, Y. Tang, R. Ballarini, W.W. Gerberich, and J. Mitchler, *Adv. Funct. Mater*., **19**, 2439 (2009).
5G. Xu and C. Zhang, *J. Mech. Phys. Solids*, **51**, 1371 (2003).
6P.R. Howie, S. Korte, and W.J. Clegg, *J. Mater. Res.*, **27**, 141 (2012).
7W.M. Mook, C. Niederberger, M. Bechelany, L. Phillippe, and J. Michler, *Nanotechnology*, **21**, 05570 (2010).
8H. Bei, S. Shim, G.M. Pharr, and E.P. George, *Acta Mater*., **56**, 4762 (2008).
9F. Östlund, P.R. Howie, R. Ghisleni, S. Korte, K. Leifer, W.J. Clegg, and J. Michler, *Philos. Mag*. **91**, 1190 (2011).
10S. Montagne, S. Pathak, X. Maeder, and J. Michler, *Ceram Int*. **40**, 2083 (2014).
11M.D. Uchic, D.M. Dimiduk, J.M. Florando, and W.D. Nix, *Science*, **305**, 986 (2004).
12D.M. Dimiduk, M.D. Uchic, and T.A. Parthasarathy, *Acta Mater*., **53**, 4065 (2005).
13J.R. Greer, W.C. Oliver, and W. Nix, *Acta Mater.*, **53**, 1821 (2005).
14O.A. Ruano, J. Wadsworth, and O.D. Sherby, *Acta Mater*. **51**, 3617 (2003).
15A. Dominguez-Rodriguez, F. Gutierrez-Mora, M. Jimenez-Melendo, J.L. Routbort, and R. Chaim, *Mater. Sci. Engr. A*. **302**, 154 (2001).
16J. Akedo and H. Ogiso, *JTST*, **17**, 181 (2008).
17J. Akedo. *JTTEE5*, **17**, 181 (2007).
18J. Akedo, *J. Am. Ceram. Soc*., **89**, 1834 (2006).
19Y. Imanaka, N. Hayashi, M. Takenouchi, and J. Akedo, *Proc. of Ceramic Interconnect and Ceramic Microsystems Technologies*, 2006.
20Y. Imanaka, N. Hayashi, M. Takenouchi, and J. Akedo, *J. Euro. Ceram. Soc*. **27**, 2789 (2007).
21Y. Kawakami, H. Yoshikawa, K. Komagata, and J. Akedo, *J. Crys. Growth*. **275**, el295 (2005).
22J. Akedo and M. Lebedev, "Piezoelectric Properties and Poling Effect of Pb(Zr, Ti)O_3 Thick Films Prepared for Microactuators by Aerosol Deposition," *Appl. Phys. Lett*. 77, 2000, p. 1710.
23S. Sugimoto, T. Maeda, R. Kobayashi, J. Akedo, M. Lebedev, and K. Inomata, *IEEE Trans. Magnetics.* **39**, 2986 (2003).
24S. Sugimoto, T. Maki, T. Kagotani, J. Akedo, and K. Inomata, *J. Magn. Magn. Mater*. **290-291**, 1202 (2005).
25H. park, J. Kwon, I. Lee, and C. Lee, *Scripta Materialia*, **100**, 44 (2015).
26M. Schubert, J. Exner, and R. Moos, *Materials,* **7**, 5633 (2014).
27D.W. Lee and S.M. Nam, *J. Ceram. Process. Res*. **11**, 100 (2010).
28S.H. Cho and Y.J. Yoon, *Thin Solid Films*, **547**, 91 (2013).
29Y.J. Heo H.T. Kim, K.J. Kim, S. Nahm, Y.J. Yoon, and J. Kim, *Appl. Therm. Eng*. **50**, 799 (2013).
30J. Exner, P. Fuierer, and R. Moos, *J. Am. Ceram. Soc*. **98**, 717 (2015).
31W.E. Lee and K.P.D. Lagerlof, *J. Electron Microscopy Technique*. **2**, 247 (1985).
32J.D. Snow and A.H. Heuer , *J. Am. Ceram. Soc.*, **56**, 153 (1973).
33M.L. Kronberg , *Acta Metall.*, **5**, 508 (1957).
34A.H. Heuer , *Phil. Mag*., **13**, 379 (1966).
35*Deformation of Ceramic Materials* edited by R.C. Bradt and R.E. Tressler (Plenum Press, New York, 1975)
36N.I. Tymiak and W.W. Gerberich, *Phil. Mag*., **87**, 5143 (2007).
37N.I. Tymiak and W.W. Gerberich, *Phil. Mag*., **87**, 5169 (2007).
38R. Nowak, T. Sekino, and K. Niihara, *Phil. Mag. A*, **74**, 171 (1996).
39J.D. Clayton, *Proc. Of the Royal Soc. A.,* **465**, 307 (2009).
40E.R. Dobrovinskaya, L.A. Lytvynov, and V. Pishchik, *Sapphire* (Springer, Boston, MA 2009).
41K.P.D. Lagerlof, A.H. Heuer, J. Castaing, J.P. Riviere, and T.E. Mitchell, *J. Am. Ceram. Soc.*, **77**, 385 (1994).
42A. Nakamura, T. Yamamoto, and Y. Ikuhara, *Acta Mater*., **50**, 101 (2002).
43T. Geipel, K.P.D. Lagerlof, P. Pirouz, and A.H. Heuer, *Acta Matall. et Mater*., **42**, 1367 (1994).
44K. Hattar, D.C. Bufford, and D.L. Buller, *Nuclear Instruments and Methods in Physics Research B*. **338**, 56 (2014).
45K. Zhen, C. Wang, Y.-Q. Cheng, Y. Yue, X. Han, Z. Zhang, Z. Shan, S.X. Mao, M. Ye, Y. Yin, and E. Ma. Nature Communications | 1:24 | DOI: 10.1038/ncomms1021
46W.M. Mook, J.D. Nowak, C.R. Perry, C.B. Carter, R. Mukherjee, S.L. Girshick, P.H. McMurry, and W.W. Gerberich, *Phys Rev B*, 75, 2007, pp. 214112-1-10.
47*Materials Science and Engineering Serving Society* edited by R.P.H. Chang, R. Roy, M. Doyama, and S. Somiya. (Elsevier Science, The Netherlands, 1998).
48D.D. Stauffer, A. Beaber, A. Wagner, O. Ugurlu, J. Nowak, K. Andre Mkhoyan, S. Girshick, and W.W. Gerberich, Acta Mater., **60**, 2471 (2012).

Thank you,
for your attention.

Pylin Sarobol –
psarobo@sandia.gov

Sandia National Laboratories

BACK UP SLIDES

Ceramic Particle RT Deformation - Sapphire

- Deformation behavior influenced by *number of internal defects*, temperature, crystal orientation/size. Numbers of pre-existing (immobile) defect scale with size.
- In situ SEM/TEM micro-compression and Molecular Dynamics Simulations

Proposed

	Micron	Sub-micron
# Pre-existing Defects	High	Moderate
Energy Density Input	Low	Moderate
Governing Mechanism(s)	Fracture	Plasticity + Fracture
Response to Compression	Crack initiation & Propagation	Dislocation nucleation, slip, crack initiation & propagation
Compression Testing	SEM	SEM and TEM

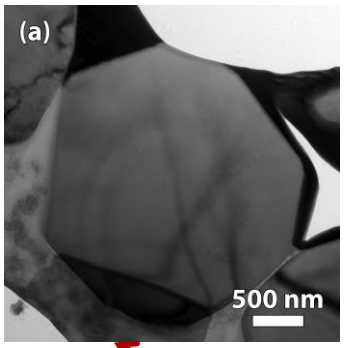

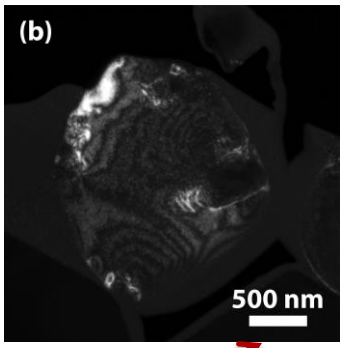

3.0μm Highly Defective

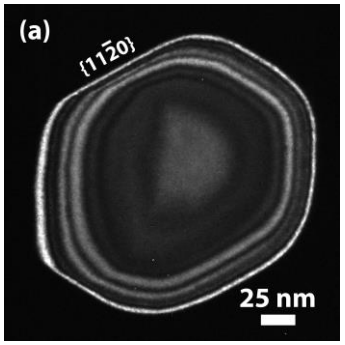

0.3μm Nearly Defect Free

- Infeasible (long computing time) to perform molecular dynamics simulations on size >0.05μm
- 'smaller' particles (0.3μm) are nearly defect-free, and 'larger' particles (3.0μm) contain immobile defects that serve as crack nucleation sites.
- Circumvented the size limitation of our models by simulating similar sized (10 nm) nanoparticles (NPs) that were either
  - single crystal
  - contained a grain boundary (GB) as an initial immobile defect.
- This approach still enables the study of NP deformation/fracture in computationally-feasible systems.

Ceramic Particle RT Deformation - Alumina

Sandia National Laboratories

- Deformation behavior influenced by *number of internal defects*, temperature, crystal orientation/size. Numbers of pre-existing (immobile) defect scale with size.
- In situ SEM/TEM micro-compression and Molecular Dynamics Simulations

Proposed

	Micron	Sub-micron	Single Crystal Nano	Bicrystal Nano
# Pre-existing Defects	High	Moderate	None	Grain Boundary
Energy Density Input	Low	Moderate	High	Low
Governing Mechanism(s)	Fracture	Plasticity + Fracture	Plasticity	Fracture
Response to Compression	Crack initiation & Propagation	Dislocation nucleation, slip, crack initiation & propagation	Dislocation nucleation, Slip	Crack initiation & propagation
Compression Testing	SEM	SEM and TEM	MD Simulation	MD Simulation

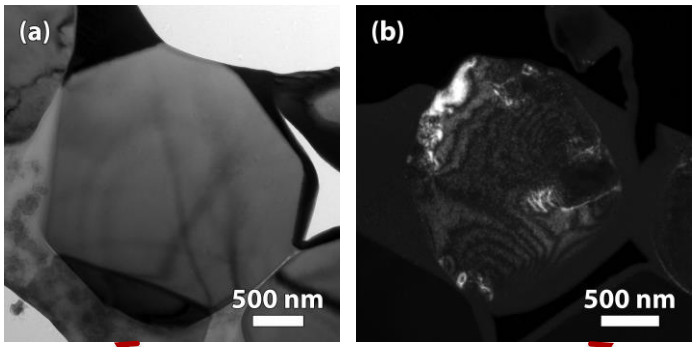

3.0μm Highly Defective

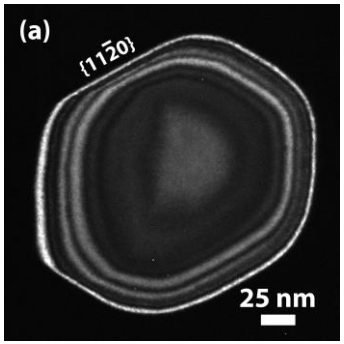

0.3μm Nearly Defect Free

Spherical Particles

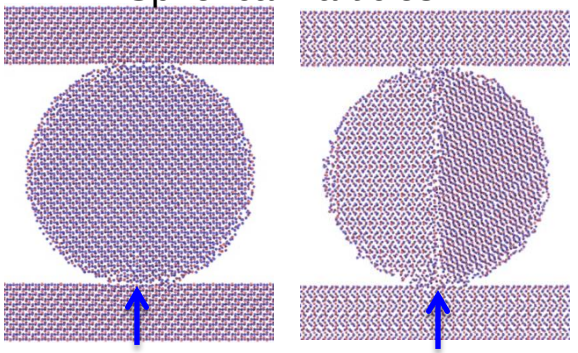

10 nm Defect Free

10 nm with a GB

In Situ SEM micro-compression – 3.0 µm

Sandia National Laboratories

Displacement control, Strain rate ~ 0.003 s^{-1}

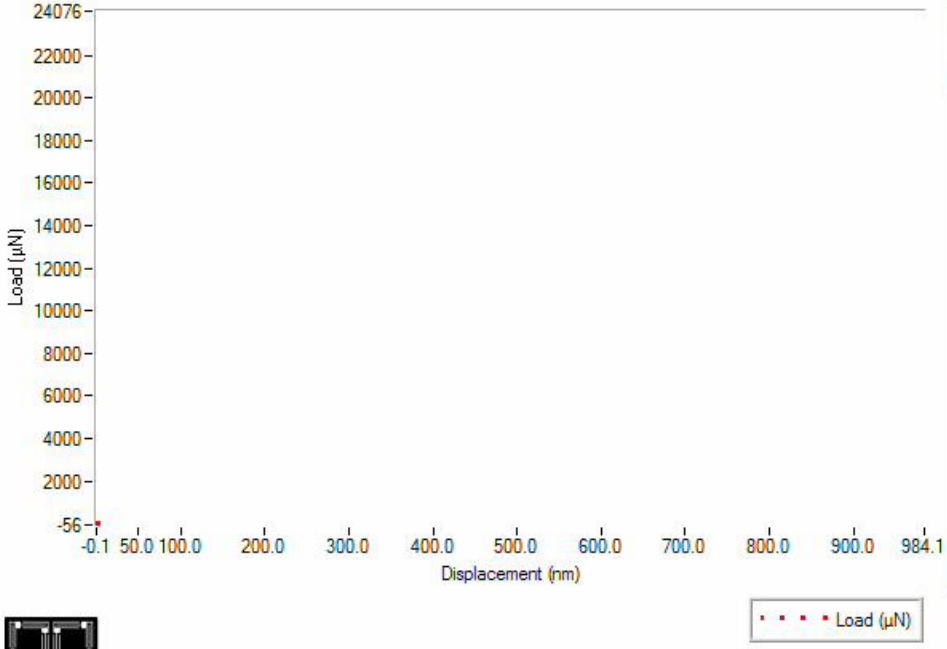

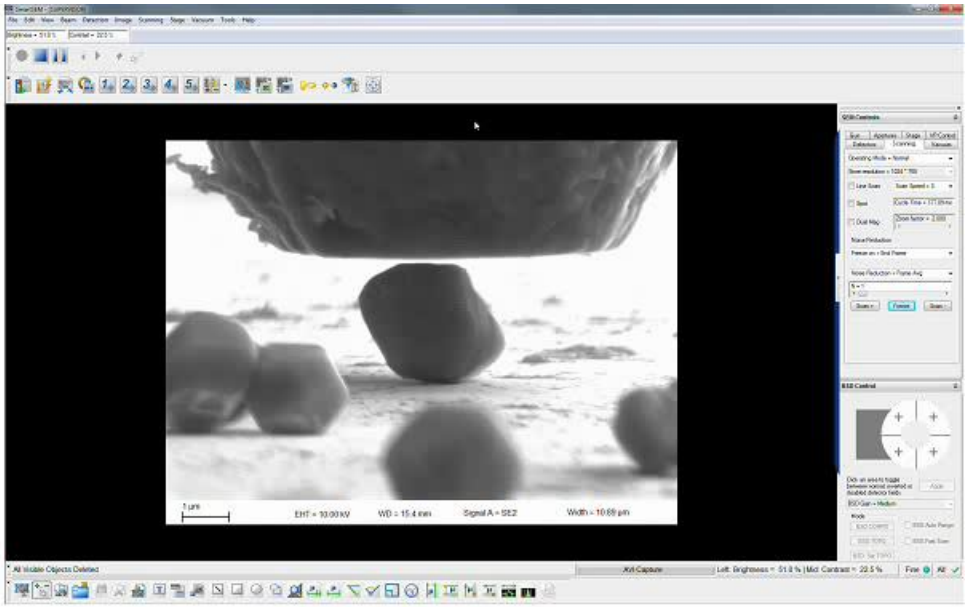

HYSITRON™

- Compressed 4 particles
- No observable shape change prior to fracture and fragmentation
- Displacement excursion corresponded to a fast fracture event
- Strain Energy Density before Fracture ~203 MJ/m^3
- Strain at fracture ~7%

Tip could not keep up with large displacement gained during fracture.

In Situ SEM micro-compression – 0.3 µm

Sandia National Laboratories

Displacement control, Strain rate ~ 0.05 s^{-1}

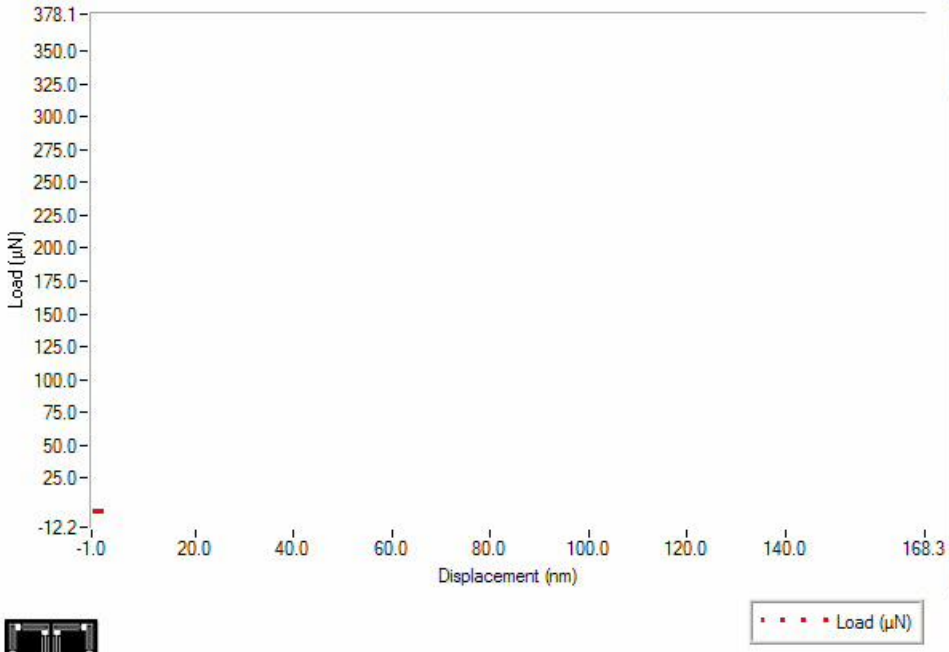

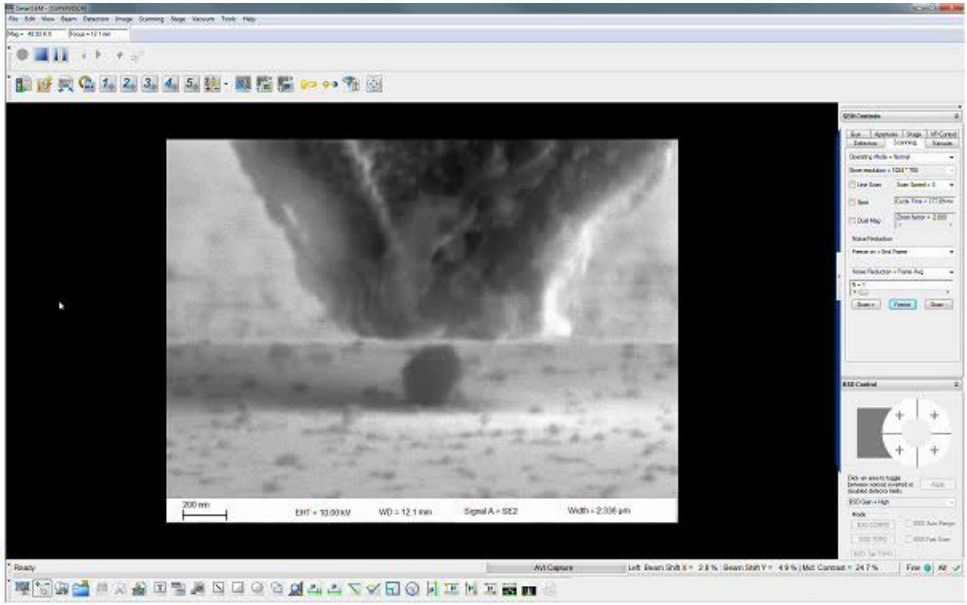

HYSITRON™

- Compressed 4 particles
- Significant plastic deformation/ shape change and stayed intact
- Displacement excursion corresponded to??? *Ex situ* observation
- Strain Energy Density before displacement excursion ~675 MJ/m^3
- Strain at displacement excursion ~16%

Tip could not keep up with large displacement gained during fracture.

Ex Situ SEM observation – 0.3 µm

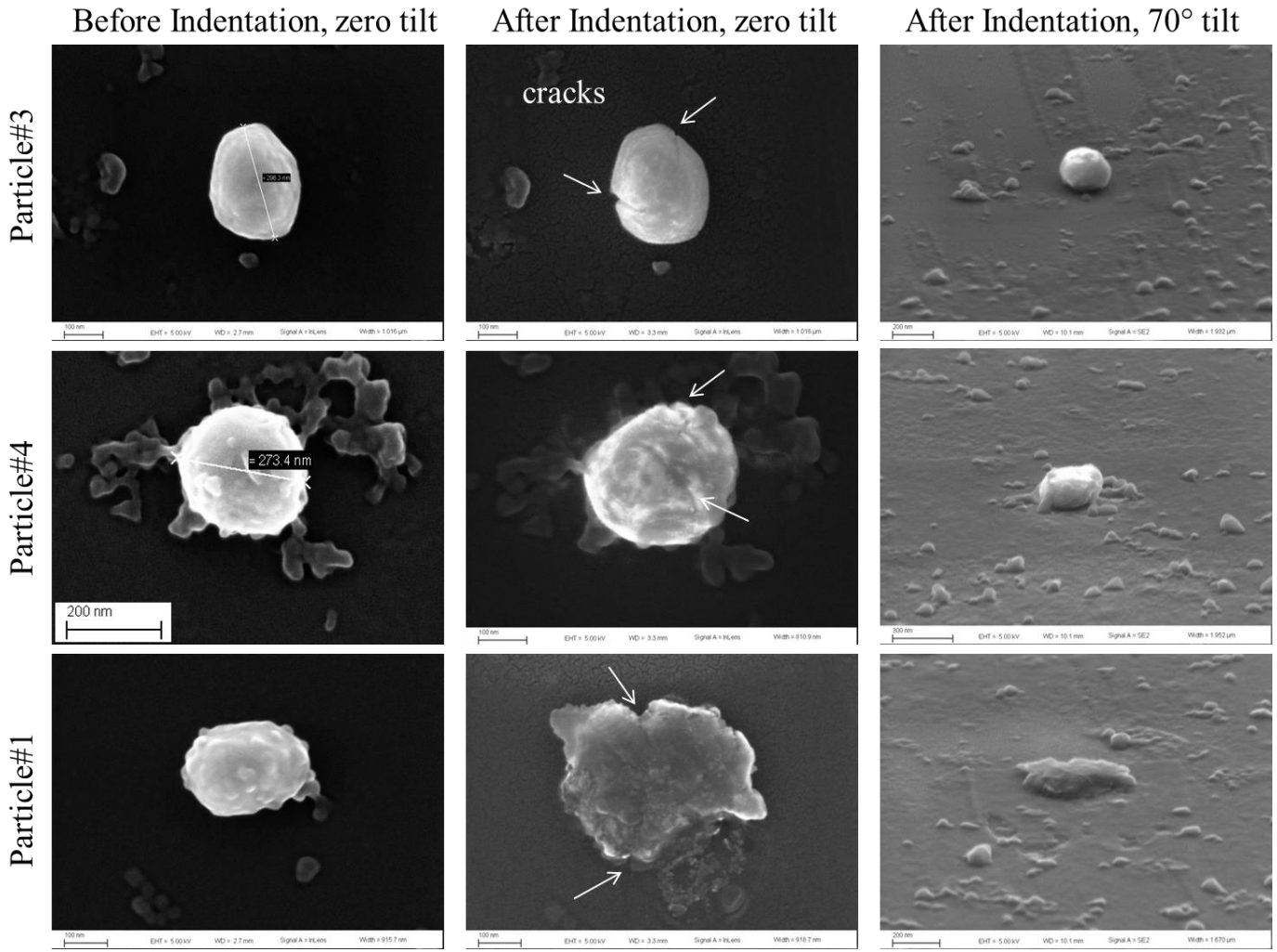

~307 µN
Max load

~420 µN
Max load

Extreme
Loading

Different deformation behavior and load at first fracture may differ from particle-to-particle due to orientation differences and different pre-existing defect densities. However, overall, the sub-micron sized alumina particles exhibited significant plastic deformation before fracture.

Micro-compression Summary

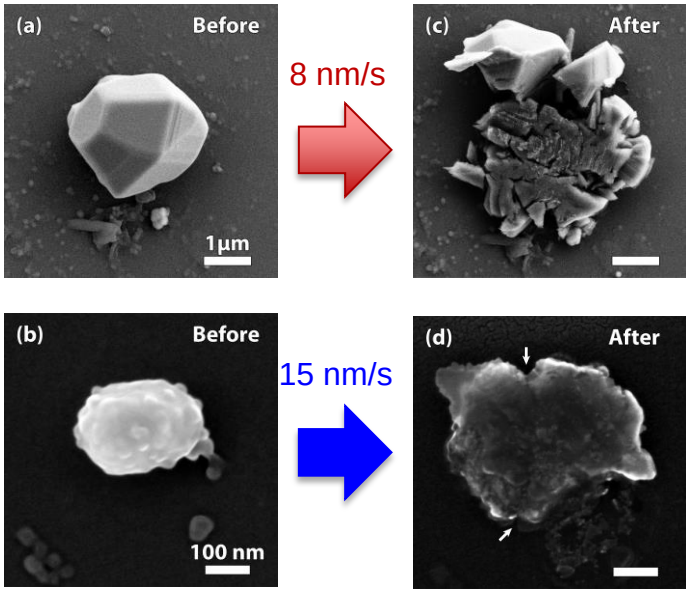

Particle Identifier	Diameter (µm)	Nominal Strain Rate (s^{-1})	Strain Energy Density Before Displacement Excursion (MJ/m^3)	Strain at displacement excursion (%)
Large Particles				
SEM-LP1	2.9	0.03	47	5
SEM-LP2	2.6	0.006	106	5
SEM-LP4	2.9	0.005	70	5
SEM-LP5	2.9	0.003	203	7
Avg Large Particles	**2.8**	-	**106±69**	**5.5 ± 1**
Small Particles				
SEM-SP2	0.17	0.09	494	11
SEM-SP3	0.29	0.05	366	12
SEM-SP4	0.28	0.05	607	13
SEM-SP5	0.29	0.05	675	16
*TEM-SA2	0.38	*0.005	573	32
*TEM-SB1	0.24	*0.009	1066	27
Avg Small Particles	**0.26**	-	**630±238**	**18 ± 9**

	Micron	Sub-micron
# Pre-existing Defects	High	Moderate
Energy Density Input	Low	Moderate
Governing Mechanism(s)	Fracture	Plasticity + Fracture
Response to Compression	Crack initiation & Propagation	Dislocation nucleation, slip, crack initiation & propagation

- Micron sized particles - brittle fracture
- Sub-micron sized particles - substantial plastic deformation before fracture and/or coordinated shear deformation.
  - **6x** higher strain energy density input
    - dislocation nucleation
  - **3x** higher accumulated strain
  - In some cases, became polycrystalline.

Ceramic Particle RT Deformation - Alumina

- Deformation behavior influenced by numbers of internal defects, orientation, size.

Verified

	Micron	Sub-micron	Single Crystal Nano	Bicrystal Nano
# Pre-existing Defects	High	Moderate	None	Grain Boundary
Energy Density Input	Low	Moderate	High	Low
Governing Mechanism(s)	Fracture	Plasticity + Fracture	Plasticity	Fracture
Response to Compression	Crack initiation & Propagation	Dislocation nucleation, slip, crack initiation & propagation	Dislocation nucleation, Slip	Crack initiation & propagation
Compression Testing	SEM	SEM and TEM	MD Simulation	MD Simulation

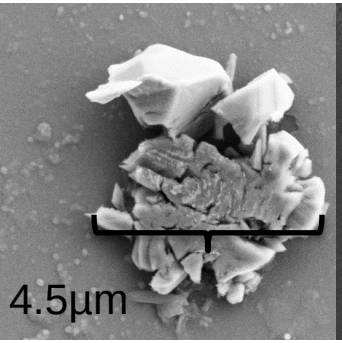

3.0µm - Fracture and Fragmentation

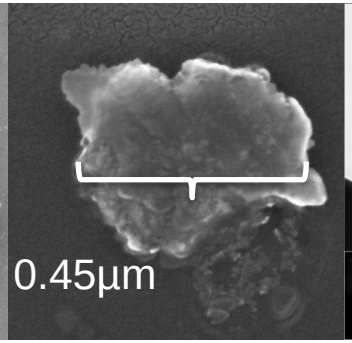

0.3µm – plastic deformation, shape change, cracking

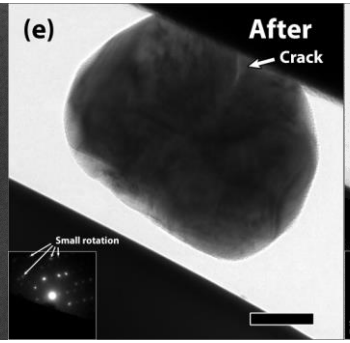

0.3µm - Dislocation Plasticity & through particle fracture

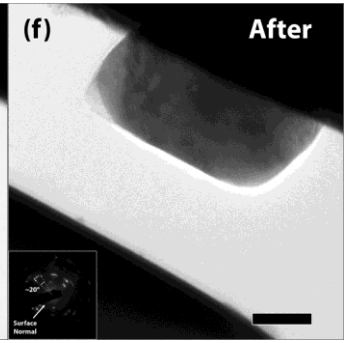

0.3µm - Coordinated Shear Deformation - Polycrystalline

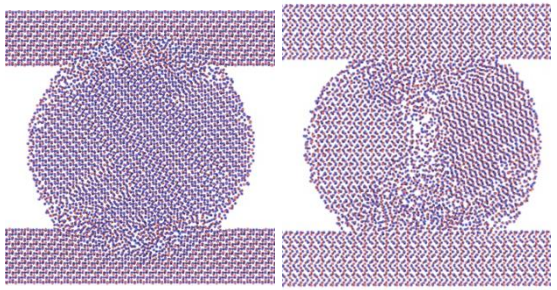

10 nm - Coordinated **10 nm - Fracture**
Shear Deformation

MD Simulation Results

10 nm diameter, contain a GB, 'Janus' α-alumina,
20 m/s, left side randomly oriented and right side compression axis ⊥ (0001) → Fracture